Available online at www.sciencedirect.com
SCIENCE DIRECT®
ELSEVIER
European Journal of Mechanics B/Fluids 23 (2004) 181–188
EUROPEAN JOURNAL OF MECHANICS B/FLUIDS

DNS and experiments of flow past a wired cylinder at low Reynolds number

S. Sirisup [a], G.E. Karniadakis [a,*], N. Saelim [b], D. Rockwell [b]

[a] *Division of Applied Mathematics, Brown University, Providence, RI, 02912, USA*
[b] *Department of Mechanical Engineering, Lehigh University, Bethlehem, PA, 18015, USA*

Received 24 April 2003; accepted 24 April 2003

Abstract

We have performed high resolution direct numerical simulations (DNS) at Reynolds number $Re = 50$, 160 and 500 for flow past a wired cylinder. Comparisons with companion PIV measurements made at $Re = 160$ validate the DNS results. It is found that at $Re = 160$ and $Re = 500$ vortex shedding is suppressed substantially while the drag force decreases compared to a smooth cylinder flow.

1. Background and objectives

Cylinders with three-dimensional surface nonuniformities occur in a variety of practical configurations, e.g., stranded cables. Furthermore, nominally smooth cylinders are often wound with a helical wire pattern, in order to attenuate the unsteady lift. The first systematic work on cylinders with helical strakes was conducted in [1]. In [2], the helical strakes successfully reduced the vibrations of large stacks in air. With regards to the optimum pitch for the strakes, it has been suggested that an effective value is $5D$, where D is the diameter of the cylinder, see [3]. Also, in [4] it was reported that the optimum thickness of the strakes is $0.08D$. The same results are obtained if strakes are replaced by wires. Much earlier, in [5] the effectiveness of a helical wire pattern was demonstrated in the supercritical Reynolds numbers range for an elastically mounted cylinder. In this configuration four wires with the thickness of $0.04D$ were wrapped helically around the cylinder with $8D$ and $16D$ pitch. The induced vibration was almost vanished and the drag coefficient was also reduced. In [6], the optimum pitch and diameter for the three and four helical wires are reported to be between $8D$ and $16D$, $D/16$ and $D/8$, respectively.

Whereas all of the aforementioned investigations have focused on determination of the loading characteristics as a function of the helical patterns of strakes or wires, in [7] a preliminary investigation is reported of the flow structure in the near-wake of the cylinder with a helical winding of $0.10D$ using a quantitative imaging technique. The emphasis of this investigation was on the instantaneous patterns of vorticity in the near-wake at a relatively high value of Reynolds number $Re = 10\,000$.

Generally speaking, little is known of the quantitative structure of the near-wake of a circular cylinder with a helical surface winding, especially at low Reynolds number, of the order of 200 or less, where deterministic processes of transition occur in the wake of a cylinder with a smooth surface, as summarized in [8]. To the best of our knowledge, there are no direct numerical simulations for a cylinder with helical strakes or a helical wired cylinder performed so far.

In this work, we aim to investigate the flow past a helical wired cylinder focusing on the flow structure as well as on computing accurately details of the body forces. To this end, we employ spectral DNS at $Re = 50$, 160 and 500 and PIV

* Corresponding author.
E-mail address: gk@dam.brown.edu (G.E. Karniadakis).

0997-7546/$ – see front matter
doi:10.1016/j.euromechflu.2003.04.003

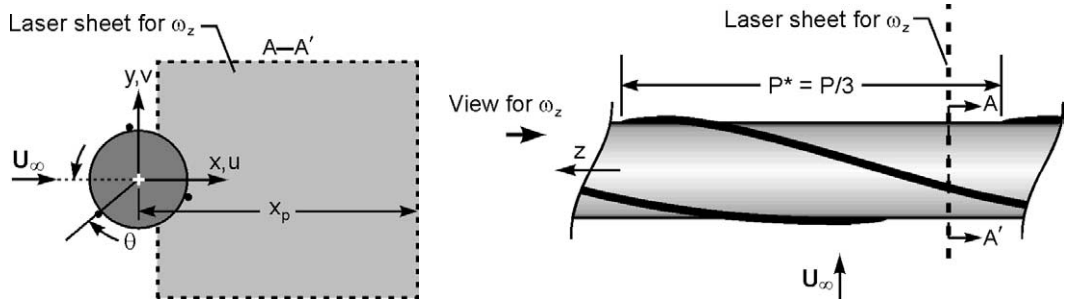

Fig. 1. Schematics of cylinder with helical winding and laser sheet for quantitative imaging.

measurements at $Re = 160$. We compare the obtained DNS results with the companion experimental data and also with corresponding results for smooth cylinders.

2. Description of experiments

In order to provide a well-posed inflow, experiments were undertaken in a free-surface water channel, which had a primary test section 914 mm wide, 968 mm deep, and 4,572 mm long. In order to attain a value of free-stream turbulence intensity less than 0.1% in the test section, it was preceded by a settling chamber, a flow conditioning system, and a contraction. Fig. 1 shows the cylinder with a helical surface winding. Also illustrated are the location and orientation of the laser sheet employed for quantitative imaging. The cylinder had a length of 508 mm and a diameter of 6.35 mm. The corresponding value of Reynolds number *Re* based on diameter D was 160. The helical wire diameter was $d = 0.39$ mm, thereby giving a diameter ratio of $d/D = 0.06$. The wire pattern took the form of a three-start helix, with an overall pitch $P = 76.2$ mm and a local pitch $P_* = 25.4$ mm. The cylinder was oriented vertically, such that it was bounded by the free-surface at its upper end and by a plate at its lower end.

Fig. 1 indicates the effective incidence angle of the local cross-sectional cut of the helical wire pattern. A cross-sectional view of the helical pattern about the cylinder is defined in relation to the orientation of the laser sheet for characterization of spanwise vorticity z. The field of view in the plane of the laser sheet is designated by the shaded area. For the present set of experiments, sectional patterns of streamlines, in addition to other flow quantities, are characterized for a range of incidence angle.

Instantaneous, quantitative patterns of the flow structure were provided by a digital technique of high-image-density particle image velocimetry. Suspended particles, in the form of metallic-coated, hollow plastic spheres (14 micron diameter) were illuminated by a dual pulsed Yag laser system, which had an output of 90 mJ per pulse. The laser sheet was generated using a combination of cylindrical and spherical lenses. Patterns of particle images were recorded by a high resolution, megapixel camera. Patterns of instantaneous velocity vectors were generated using a cross-correlation technique between successive frames of particle image patterns. For the images herein, the interrogation window had a size 32 pixels × 32 pixels. An effective overlap of 50% was used in order to satisfy the Nyquist criterion.

3. Numerical simulations

The wired cylinder studied has geometry as shown in Fig. 2. Specifically, three wires are wrapped in the shape of triple helix around the cylinder with the pitch of $12D$. The angle between each wire is $\pi/3$ and the width of the wires, d, is $D/16$, where D is the diameter of the cylinder. The length of the cylinder, L, is $4D$, which is the minimum possible length that can accommodate periodic boundary conditions in the spanwise direction. The geometry parameters have been based on the experiments described in the previous section.

A computational domain with the dimensions $40D \times 60D \times 4D$ (crossflow–streamwise–spanwise) has been used. Tetrahedral meshes have been generated by Gridgen, a commercial software, and we have imposed the periodicity in the boundary condition in y (crossflow) and z (spanwise) direction. Dirichlet inflow and Neumann outflow boundary conditions are imposed in x direction.

For comparison, we also simulated two-dimensional and three-dimensional flow past smooth circular cylinder using triangular meshes. For $Re = 500$ we employ Fourier expansions along the spanwise direction.

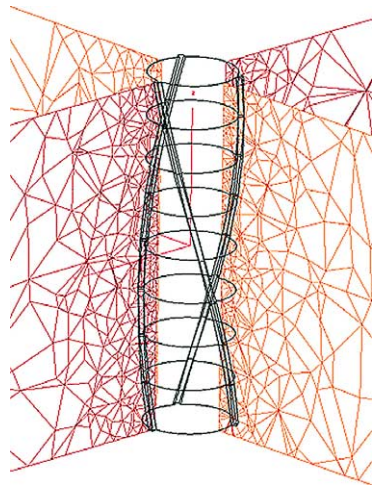

Fig. 2. Subregion of tetrahedral mesh (flat wire-frame) of the wired circular cylinder; only one-third of the pitch is simulated.

The flow field is obtained by solving the two- and three-dimensional, unsteady Navier–Stokes equations for the smooth and wired case, respectively. These equations are solved using the spectral/hp element method [9], with the number of elements for the wired cylinder being 17 890 tetrahedra and 412 triangular elements for the smooth case. The order of polynomial basis is varied from third to seventh for the three-dimensional runs. Also, polynomial of order seventh is used for two-dimensional runs. For the Fourier simulations we use polynomial with fifth order in xy-plane and we expand along the z direction using 32 Fourier modes.

We compute the viscous and pressure forces at every point on the cylinder surface and also in time from :

$$F_v^{\text{drag}} = -\oint \mu\left(2\frac{\partial u}{\partial x}n_x + \left(\frac{\partial u}{\partial y}+\frac{\partial v}{\partial x}\right)n_y + \left(\frac{\partial u}{\partial z}+\frac{\partial w}{\partial x}\right)n_z\right)\mathrm{d}s, \qquad F_p^{\text{drag}} = \oint pn_x\,\mathrm{d}s,$$

$$F_v^{\text{lift}} = -\oint \mu\left(2\frac{\partial v}{\partial y}n_y + \left(\frac{\partial u}{\partial y}+\frac{\partial v}{\partial x}\right)n_x + \left(\frac{\partial v}{\partial z}+\frac{\partial w}{\partial y}\right)n_z\right)\mathrm{d}s, \qquad F_p^{\text{lift}} = \oint pn_y\,\mathrm{d}s,$$

where n_x, n_y, n_z represent the outer unit normal pointing outward. The aforementioned forces are then normalized as

$$C_{Dp} = \frac{F_p^{\text{drag}}}{\frac{1}{2}\rho U_\infty^2 DL}, \quad C_{Dv} = \frac{F_v^{\text{drag}}}{\frac{1}{2}\rho U_\infty^2 DL}, \quad C_{Lp} = \frac{F_p^{\text{lift}}}{\frac{1}{2}\rho U_\infty^2 DL}, \quad C_{Lv} = \frac{F_v^{\text{lift}}}{\frac{1}{2}\rho U_\infty^2 DL},$$

which give the pressure drag coefficient, viscous drag coefficient, pressure lift coefficient and viscous lift coefficient, respectively. The total lift and drag coefficients are then defined as:

$$Cl = C_{Lp} + C_{Lv}, \qquad Cd = C_{Dp} + C_{Dv}.$$

4. Results

4.1. Resolution studies

We have performed simulations for the three-dimensional wired cylinder at Reynolds numbers 50, 160 and 500. Also, for comparison we have performed two-dimensional simulations for the *smooth cylinder* at $Re = 50$ and $Re = 160$ and three-dimensional simulations at $Re = 500$. In this case intrinsic three-dimensional effects set in at $Re \approx 180$, see [8]. The results from the case of smooth cylinder are in good agreement with [10].

In order to estimate the resolution requirements we performed systematic p-convergence studies for $Re = 50$ and for $Re = 160$ to find the best order of polynomial basis for the three-dimensional cases. Fig. 3 shows that for the case of $Re = 50$ it is sufficient to use third-order because there is not much difference on the lift coefficient. However, for the case of $Re = 160$, the appropriate order of polynomial expansion is five. For the case of Reynolds number 500, we have run the simulation with seventh order polynomial as the first runs showed that resolution with fifth order was inadequate.

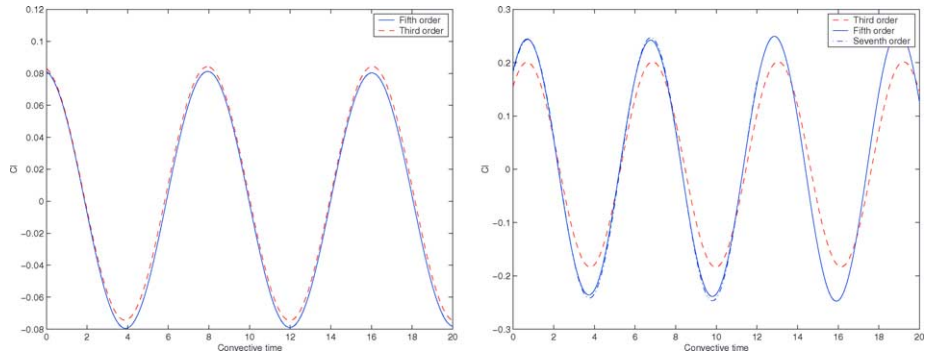

Fig. 3. Resolution studies: p-convergence for Reynolds number at 50 (left) and Reynolds number at 160 (right) by varying the polynomial order. Lift coefficient versus time.

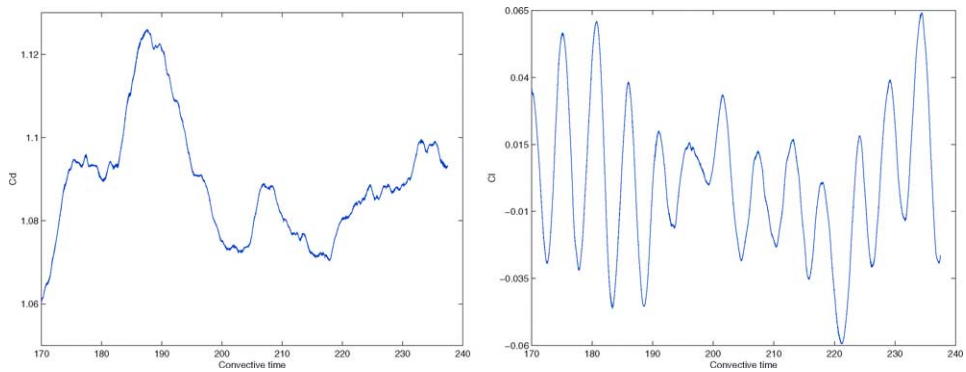

Fig. 4. Drag (left) and lift (right) coefficient at Reynolds number 500.

4.2. Comparison with experiments

We first compare snapshots from DNS to the experimental data at $Re = 160$ at various planes. We note here that in the experiment the strakes are wires with circular cross-section of diameter $D/16$ but in the simulations the strakes have square cross-section for computational convenience. Despite these differences, we see in Fig. 5 that the structures of the flow past wired cylinder at each z-plane obtained from DNS simulation are in good agreement with the ones obtained from the experiments.

4.3. Lift and drag forces

The drag and lift coefficients for all cases we have simulated are summarized in Figs. 6 and 7, respectively. From the lower plot in Fig. 6, we see that the viscous drag coefficient depends strongly on the Reynolds numbers. In contrast, the middle plot shows that the pressure drag coefficient depends on both the geometry of the bluff body and the Reynolds numbers. We can see that at a lower Reynolds number the pressure drag from the wired cylinder is greater than that from the smooth one, but at higher Reynolds number the pressure drag for the wired cylinder is lower than that for the smooth cylinder.

Also, as we see in the middle and buttom plots of Fig. 7, at the low Reynolds numbers the viscous and pressure lift coefficients have about the same magnitude for both the smooth and wired cylinders. However, at Reynolds number 160, the lift coefficient

Table 1
Strouhal number extracted from the spectrum of lift coefficients of the smooth and wired cylinder

Reynolds numbers	Smooth cylinder	Wired cylinder
50	0.13	0.12
160	0.19	0.16
500	0.22	0.17

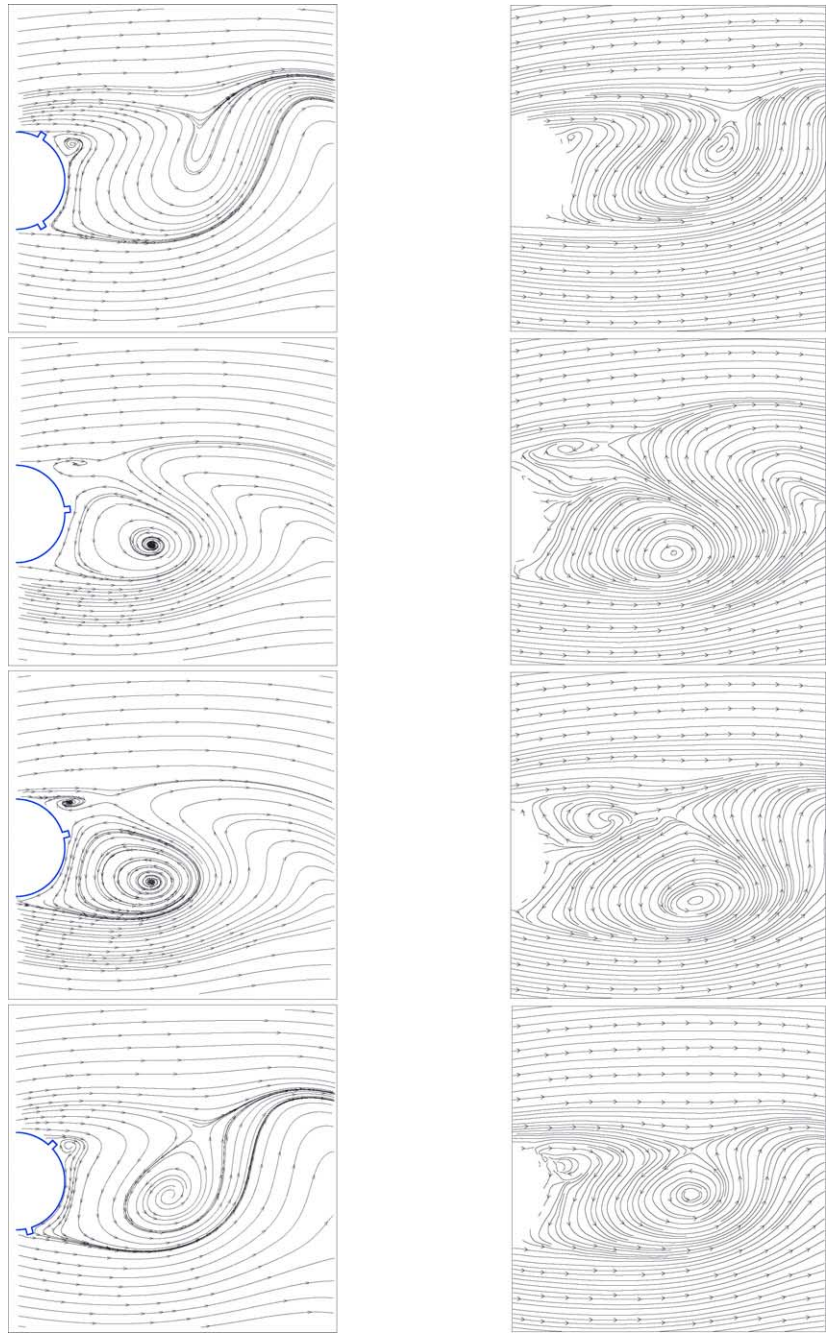

Fig. 5. Comparison for a snapshot with phase averaged data at difference z-planes of DNS (left) and experiment (right). From top to bottom: $\theta = 0^\circ$, $\theta = 65^\circ$, $\theta = 75^\circ$, $\theta = 105^\circ$.

from the wired case decreases dramatically, with peak-to-peak values of 0.5 but for the smooth case, the peak-to-peak value is about 1.16. These results demonstrate that the magnitude is decreased by 2.3. Moreover, at Reynolds number 500, the lift coefficient magnitude of the wired case is about 0.12 while that of smooth cylinder is 2.4, this shows substantial suppression of the lift forces, i.e., about 20 times decrease.

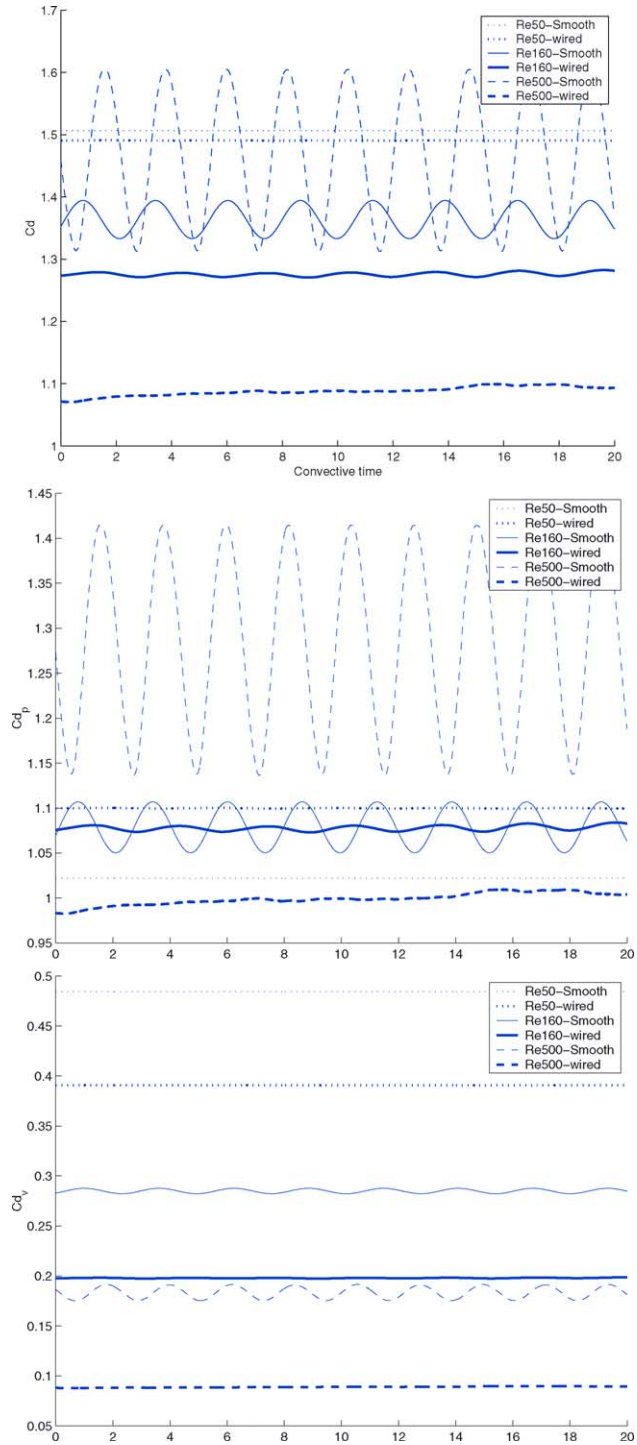

Fig. 6. From top to bottom: coefficients of total drag, pressure drag and viscous drag.

The results from the spectrum analysis of the lift coefficients for each case are summarized in Table 1. The lower Strouhal number values of the wired cylinders are also suggestive of the suppression effect that the wires have. The spectrum of the lift and drag coefficients for the case of Reynolds number 500 contain other incomensurate frequencies and appear quasi-periodic (see Fig. 4).

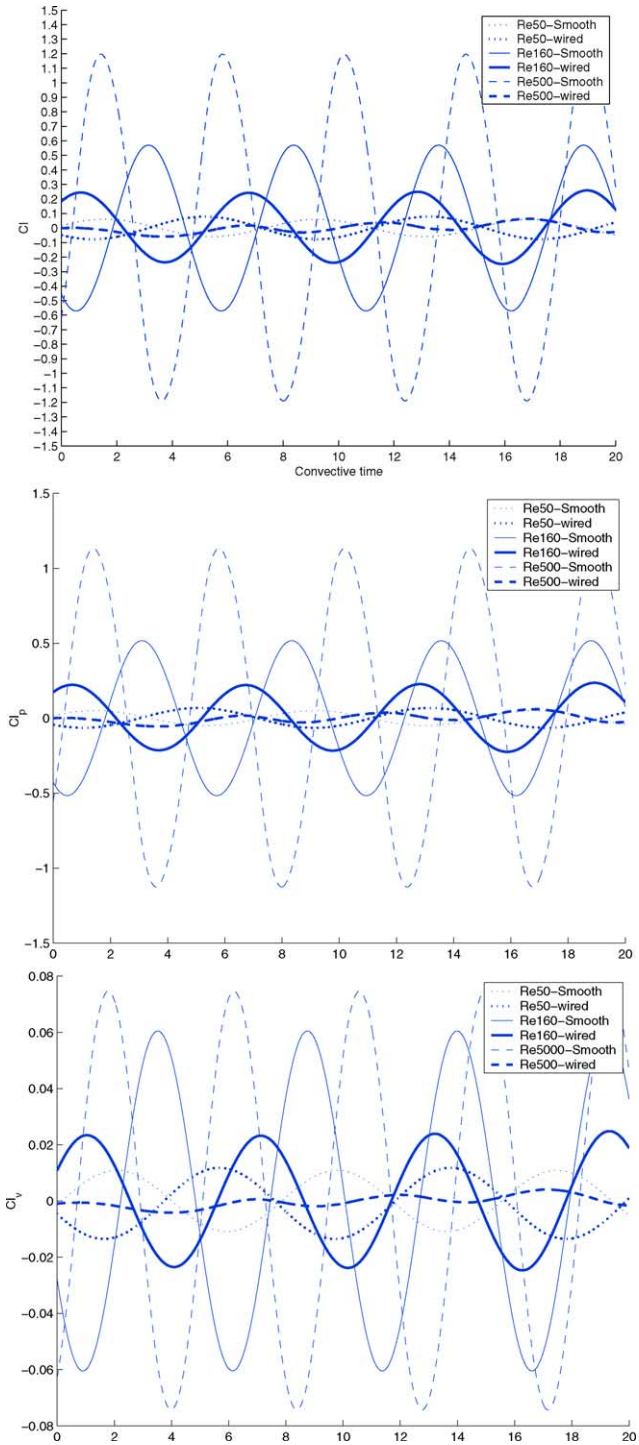

Fig. 7. From top to bottom: coefficients of total lift, pressure lift and viscous lift.

5. Summary

We have presented here, for the first time, numerical and experimental results at low Reynolds number for wired cylinders. Comparison of the near-wake flow structures shows good agreement for the test case of $Re = 160$. The DNS results show that for this range of Reynolds number both drag and lift coefficients are decreased compared to the corresponding values of flow past smooth circular cylinder.

References

[1] C. Scuton, D.E. Walshe, A means of avoiding wind-excited oscillations of structures with circular or nearly circular cross-section. Nat. Phys. Lab., UK Aero Rep. No 335, 1957.
[2] D.E. Walshe, L.R. Woolton, Preventing wind induced oscillations of structures of circular section, in: Proc. Inst. Civil Engrs, 1970.
[3] E. Naudascher, D. Rockwell, Flow-Induced Vibrations An Engineering Guide, Balkema, 1994.
[4] H. Ruscheweyh, Measures to control dangerous stack vibrations, Mitteilung Curt-Risch-Institut, Techn. Germany, 1978, p. 519.
[5] K. Nakagawa, T. Fujino, Y. Arita, Y. Ogata, K. Masaki, An experimental investigation of aerodynamic instability of circular cylinders at supercritical reynolds numbers, in: Ninth Japanese Congress of Applied Mechanics, 1959, p. 235.
[6] W. Weaver, Wind-induced vibrations in antenna members, ACSE J. Engrg. Mech. Division 87 (1961) 141–165.
[7] C.K. Chyu, D. Rockwell, Near-wake flow structure of a cylinder with a helical surface perturbation, J. Fluids Structures 16 (2) (2002) 263–269.
[8] C.H.K. Williamson, Vortex dynamics in the cylinder wake, Annu. Rev. Fluid Mech. 28 (1996) 477–539.
[9] G.E. Karniadakis, S.J. Sherwin, Spectral/hp Element Methods for CFD, Oxford University Press, 1999.
[10] R.D. Henderson, Details of the drag curve near the onset of the vortex shedding, Phys. Fluids 7 (9) (1995) 2102–2104.